RESIDUAL PYRAMID FCN FOR ROBUST FOLLICLE SEGMENTATION

Zhewei Wang[1]   *Weizhen Cai*[1]   *Charles D. Smith*[2]   *Noriko Kantake*[3]   *Thomas J. Rosol*[3]   *Jundong Liu*[1]

[1]School of EECS, Ohio University, Athens, OH 45701
[2] Department of Neurology, University of Kentucky, Lexington, KY 40508
[3] Department of Biomedical Sciences, Ohio University, Athens, OH 45701

ABSTRACT

In this paper, we propose a pyramid network structure to improve the FCN-based segmentation solutions and apply it to label thyroid follicles in histology images. Our design is based on the notion that a hierarchical updating scheme, if properly implemented, can help FCNs capture the major objects, as well as structure details in an image. To this end, we devise a residual module to be mounted on consecutive network layers, through which pixel labels would be propagated from the coarsest layer towards the finest layer in a bottom-up fashion. We add five residual units along the decoding path of a modified U-Net to make our segmentation network, Res-Seg-Net. Experiments demonstrate that the multi-resolution set-up in our model is effective in producing segmentations with improved accuracy and robustness.

1. INTRODUCTION

Thyroid is the largest endocrine gland in human body and it produces hormones that influence the metabolic rate and protein synthesis. Follicles make up one of the major components of thyroid glands. The morphology of follicle cells can often serve as a reliable indicator of the health status of the glands - healthy cells are usually homogeneous while cell polymorphism likely signals an abnormal mutation, from inflammations to cancers [1]. Therefore, Identification and evaluation of follicle polymorphism through histological images are of great importance for thyroid cancer diagnosis, as well as treatment planning.

Separating follicles from the surrounding tissue is often a prerequisite step for many other analysis tasks. As manual delineations are normally tedious, time-consuming and prone to intra- and inter-operator errors, various automatic solutions have been proposed in the past 20 years or so. Traditional approaches include boundary tracing [2], watershed [3], graph cuts [4], and Gaussian mixture models [5]. They commonly take certain hand-crafted features, e.g., edges or texture, as the basis for pixel labeling and subsequent analysis.

In recent years, deep neural networks have emerged as a new and more powerful paradigm, which revolutionized many artificial intelligence areas, including semantic segmentation. Fully convolutional network (FCN) [6] and its variants, including U-Net [7], produce state-of-art results on many data and applications. The success of FCNs should be attributed, in great part, to their capability of processing input images at different spatial scales. FCNs are commonly constructed with an encoder-decoder architecture. In the encoding path, input images are processed through a number of convolution + pooling layers to generate high-level latent features, which are then progressively upsampled in the decoder to reconstruct the target pixel labels.

A crucial issue in FCN design is how to effectively integrate the feature maps produced in higher (finer) layers and those in lower (coarser) layers. The former are richer in semantics, while the latter carry more spatial details that define class boundaries. Early efforts lead to the developments of skip architecture [6], bridges with feature concatenation [7], dilated convolution [8], up-down-sampling [9], among others. New models have emerged in the past two years, such as the utilizations of dilated pooling [10], supervision with additional labels [11], multi-task learning [12], multi-view ensemble [13], convolutional LSTM [14] and shape preserving loss [15]. Originated from the first FCN, most existing solutions follow a common setup: the network objective function is defined at the last layer, between its outputs and the ground-truth masks. While the features are learned and propagated along layers in a multi-scale manner, their updates are solely driven with an overall penalty defined on the final outputs. Hierarchical updates through image pyramids, proven effective in many previous studies [16], are essentially lacking in most of the existing FCN models. Zhang *et al.* [11] utilizes a multi-resolution loss, but the computation is still not conducted within a sequential update framework.

To seek a remedy, we propose a new FCN-based model in this paper and apply it to thyroid follicle segmentation. The design goal is to equip FCNs with a level-by-level hierarchical updating mechanism, hoping it will lead to more robust and accurate segmentation performance. To this end, we include additional loss terms based on low-layer feature maps to ensure a good starting segmentation at coarse levels. We also employ residual units to facilitate level-by-level segmentation refinements, when network inference is carrying out along the decoding path. With these two setups, our model can take full advantage of hierarchical multi-resolution processing.

2. METHOD

Many traditional image analysis solutions [17, 18] have demonstrated that multi-resolution representations [16] enable effective processing pipelines for both segmentation and registration tasks. In these models, input images are resampled and transformed into coarse levels in a bottom-up manner. The processed results are then propagated in a reverse top-down direction to provide the fine levels with better starting estimations, often leading to more accurate final results.

However, such bottom-up and top-down input/result transitions are absent in FCNs. No intermediate segmentation result at any coarse resolution is generated in FCNs to serve as a guidance for finer levels. The loss functions in most FCNs are defined only at their final layers, between the network predictions and ground-truth segmentations. With such losses, which put no emphasis on coarse level results, the efficacy of an end-to-end learning, especially through a network with many layers, may be greatly hindered.

These observations lead us to the development of a new FCN model. We modify the decoding layers of U-Net with an intention to impose a bottom-up structure, through which the segmentations from coarse levels can be transited and refined in fine layers. To further ensure the refinements to take place in an effective way, we adopt the residual concept [19] to design a residual module as the building block for our network. We term this module Res-Seg.
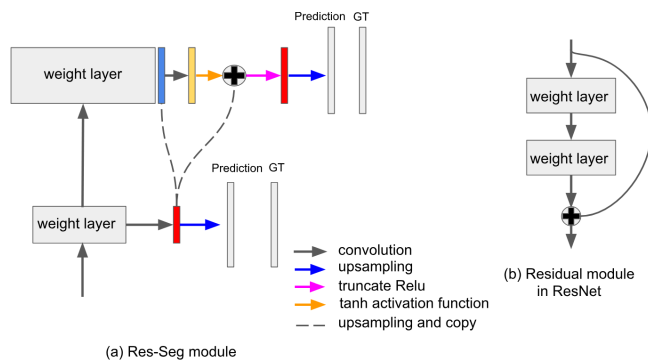
2.1. Res-Seg module

Fig. 1. (a) Res-Seg module for segmentation. Picture is best viewed in color. (b) Residual blocks proposed in ResNet [19].

Fig. 1 (a) shows a Res-Seg unit of two consecutive layers. At each layer, an intermediate probability map (prob-map), shown as a red bar, is generated and compared (after upsampling) with the ground-truth segmentation. Meanwhile, the prob-map from a low resolution layer is sent to its upper (finer) layer with two aims: 1) it will provide a good starting point for the latter; 2) it will get refined in the upper layer. To facilitate the finer layer to focus on learning the increment

details, we adopt a similar residual-connection structure from the ResNet [19] for our Res-Seg module.

As shown in Fig. 1 (a), the prob-map from the low level is upsampled (blue bar) and then sent to the high layer at two spots. Firstly, the blue bar is concatenated with the feature maps to help produce the prob-map at the finer level. The second location is on the path from the concatenated feature/prob maps to their own prob-map at the upper layer. With that, the fine layer essentially learns the residual (yellow bar) between the upsampled coarse and ground-truth segmentations. In other words, the fine layer is positioned to learn refinements for the coarse segmentation.

We have two considerations in the design of this residual unit. Firstly, the upsampled lower layer prob-map, the blue bar, has the values in the range of [0, 1]. The direct output of the upper layer, the yellow bar, which is the residual between the blue bar and the ground-truth, is in the range of [-1, 1]. With this consideration, tanh is a good choice for the activation function to be applied on the concatenated feature/prob maps. This operation is shown as a yellow arrow in Fig. 1. The second consideration is about the activation function in generating the prob-map at the upper layer. In this work, we chose a truncated ReLU, $f(x) = \max(\min(x, 1), 0)$, to map the output of this layer into the range of [0, 1].

While our Res-Seg module is inspired by the residual layers in ResNet, there are several major differences in their designs and functionalities. Firstly, our Res-Seg module is designed for segmentation and the output of each layer is supervised by the ground truth. The ResNet blocks in Fig. 1 (b), however, are not directly regulated by the ground-truth class labels. The purpose of ResNet blocks is to propagate the context information to the next layer, while our Res-Seg module aims to bring a direct guidance from the ground-truth at each layer. The second major distinction lies in the structures of the two modules. As illustrated in the last paragraph, there are several well-grounded connections and activation function setups in our res-seg, designed specifically for semantic segmentation.

Two updating schemes To ensure each upper layer to only focus on refining the results (prob-maps) sent from the previous layer, these prob-maps should be fixed at both plugging spots in the upper layers. This setup would conform to the design goal of our level-by-level updating scheme. In our implementation, the prob-map of each layer along the decoding path is copied to its upper layer, and set to untrainable there. By doing so, we force the higher layer learn the differences between the lower layer prob-map and the ground-truth. A different setting, however, can be borrowed from the ResNet, where all layers/weights are updated through back-propagation. While deviating from our level-by-level design notion, this approach certainly grants more flexibility over the learning procedure, allowing the network to minimize the total loss to its full potential. In this work, we implement both settings to compare their performance.

It should be noted that our residual module is rather general, and it can be integrated into the decoding path of many FCN networks. We choose U-Net as the baseline network for comparison and modification. We term our overall segmentation network as Res-Seg-Net.

2.2. Res-Seg-Net

We keep the overall architecture of the original U-Net, including the number of layers, in our Res-Seg-Net. Two major modifications have been made on U-Net to fit our data and task. Firstly, we reduce the number of channels at each layer, to have fewer parameters. We start with 32 channels (64 channels in U-Net), followed by doubling the number of channels at each down-sampling step along the contraction path. The expansion path is kept symmetric to the contraction path. Secondly, we use padding in every convolution operation to maintain the spatial dimension. Dimension changes only occur at polling (reduced to half) and upsampling (enlarge two times). In this way, we do not have to crop the contraction layers, as U-Net does, for skip connections.
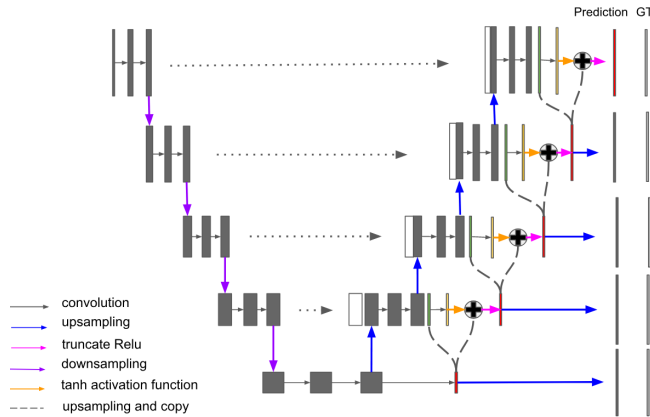

Fig. 2. Res-Seg-Net architecture. GT stands for ground-truth.

The integration of modified U-Net with our proposed Res-Seg module starts at the bottom (lowest resolution) layer of the network. Following the expansion path, our residual module is applied on each pair of adjacent upsampling layers, as shown in Fig. 2. Overall, the network produces four intermediate and one final probabilistic segmentation maps. At each layer, the intermediate segmentation map is obtained by up-sampling the respective prob-map, through a single bilinear filter, to match the dimension and resolution of the ground-truth mask.

Multi-resolution loss function We resort to Dice loss [20] to measure the difference between each segmentation map with the ground-truth mask. The choice is based on the facts: 1) Dice Similarity Coefficient (DSC) is a common metric to evaluate segmentation performance, which is also adopted in this work; 2) Dice loss has been widely used as a

differentiable approximation of DSC. Let S be the segmentation result produced by a solution and R be the ground truth. In Dice loss, segmentation S is relaxed to a probability map of real numbers between 0 and 1, and the loss is computed as:

$$\text{Dice loss} = -\frac{2\sum_i s_i r_i}{\sum_i s_i + \sum_i r_i} \quad (1)$$

where $s_i \in [0,1]$ is the label prediction at pixel i, and $r_i \in \{0,1\}$ is the corresponding binary ground truth. The overall object function in our Res-Seg-Net is defined as the summation of weighted Dice losses, which is

$$L_{Dice} = -\sum_i w_i D_i \quad (2)$$

where D_i is the Dice loss of an individual layer, and w_i is the corresponding weight. In our experiment, the weight of the Dice loss is set as 1/4 for intermediate layers, and 1 for the final layer. We give the highest resolution layer larger weight as it produces the ultimate segmentation prediction of the network.

3. EXPERIMENTS

Data To evaluate the effectiveness of our proposed Res-Seg-Net for follicle segmentation, we conducted experiments on histology slides of rat thyroid stained with hematoxylin-eosin (H & E). The images have resolution of 1μm/pixel. Ground-truth segmentations were generated based on manual delineations. A veterinary pathologist traced the boundaries of all distinguishable follicles and colloids in one particular lobe. QuPath [21] was employed to trace continuous contours, which are actually polygons. As our network processes and outputs image matrices, we converted the ground-truth segmentation from polygons to binary masks through the point-in-polygon algorithm [22].

Fixed-sized square subimages (800 × 800) were randomly sampled from the slides. Totally 100 such subimages were extracted from the original pathology slides, and together with the manual masks, they make up our data in this work. To validate our models, the 100 image-mask pairs were randomly separated into training, validation and test groups, with a size ratio of 8:1:1. In order to obtain more training samples, as well as to reduce overfitting, we further extracted smaller-sized (640 × 640) patches from the subimages, also in a random manner. The patches are also arbitrarily flipped to augment the training data. The validation set is used to select optimal hyper-parameters in our models (which is epoch number of early stopping).

Results As we mentioned in section 2.1, we intend to explore two different weight updating schemes in our Res-Seg-Net. One version is to fix upsampled prob-map after it is sent to the upper layer. We call this version Res-Seg-Net_fixed. The other setup allows all weights to be updated freely, which we term Res-Seg-Net_non-fixed.
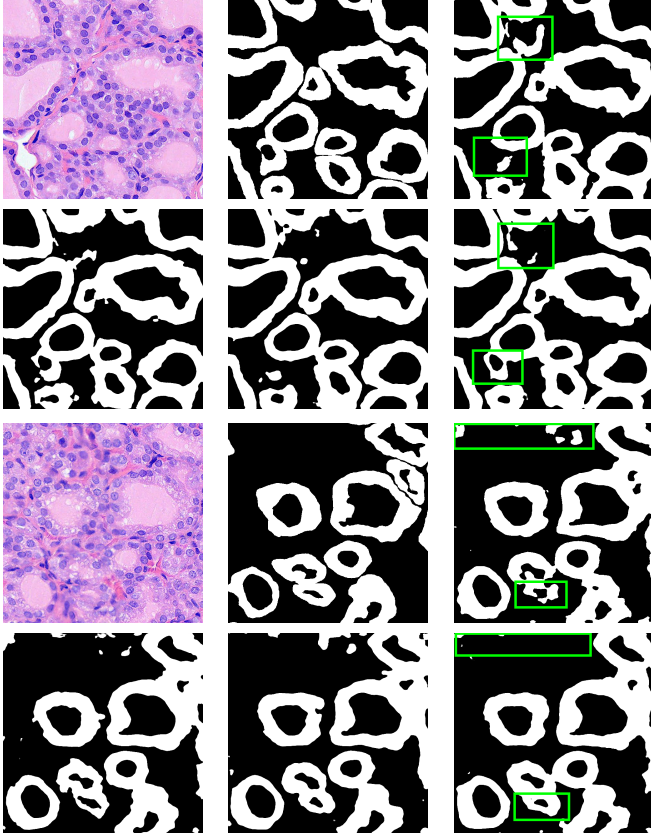
Fig. 3. Two image examples and their segmentations. First row: input image, ground-truth, and result from U-Net. Second row: results from Res-Seg-Net$_{horz}$, Res-Seg-Net$_{non\text{-}fixed}$, and Res-Seg-Net$_{fixed}$. Rows 3 and 4 show another example.

To explore the effectiveness of the notion of vertical refinements, i.e., residual updates along coarse-fine hierarchy, we also designed a solution of horizontal refinements as a competing model. More specifically, we stack five Res-Seg modules with upsampling removed, only at the last layer of the modified U-Net, which would carry out segmentation refining only along the highest resolution. We name this model Res-Seg-Net$_{horz}$. The weights updating scheme in Res-Seg-Net$_{horz}$ is the fixed version – prob-maps sent to the upper layers are all set to untrainable.

The results of the four competing models are shown in Table 1. The *Validation* column shows the best result of each

Table 1. Segmentation results on Follicles

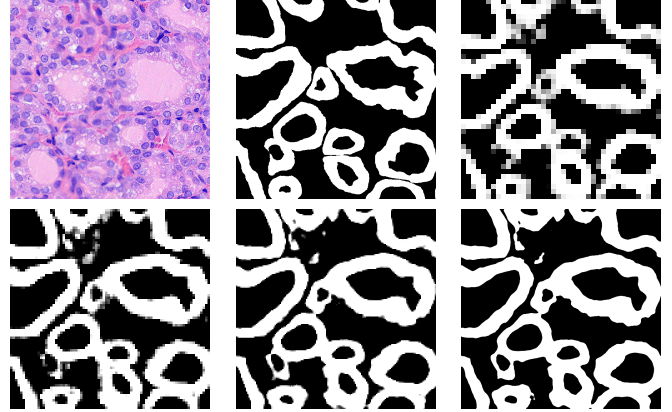| FCN	Dataset	
	Validation	**Test**
Res-Seg-Net$_{fixed}$	86.44	**85.51**
Res-Seg-Net$_{non\text{-}fixed}$	86.67	84.97
Res-Seg-Net$_{horz}$	86.19	85.23
UNet (Baseline)	86.11	84.79

Fig. 4. Segmentation results of Res-Seg-Net$_{fixed}$. Top row: input, ground-truth, first level segmentation. Bottom row: results from the second, third and fifth levels.

model on the validation set, while the *Test* column contains the results on the test dataset. The results show that all the Res-Seg based models outperform the U-Net, where Res-Seg-Net$_{fixed}$ obtained the highest DSC on the test data.

Fig. 3 shows two image examples, their ground-truth masks, and the final segmentations generated by competing models. Comparing with U-Net, Res-Seg based models generally have fewer false positives. Comparing with Res-Seg-Net$_{horz}$, Res-Seg-Net$_{fixed}$ and Res-Seg-Net$_{non\text{-}fixed}$ both generate cleaner outputs, which can serve as an evidence that hierarchical refinings are effective in improving segmentations in both accuracy and robustness. These effects can be clearly seen within the areas highlighted with green boxes.

We fed Res-Seg-Net$_{fixed}$ with the patch in the first row of Fig. 3, and output their segmentations maps of each layer in Fig. 4. The segmentation refining process is evident, as more and more details are added to the finer outputs. The low resolution segmentations tend to catch the primary shapes of the target objects. Moving upwards, they not only provide guidance for fine-resolution labelings to capture more details, but also set up certain guard to reduce the appearance of noisy spots.

4. CONCLUSIONS

The Res-Seg module proposed in this paper facilitates the multi-resolution processing of hierarchical presentations and information flow in a network. Mounted onto the expansion path of an FCN, it can help each layer focus on learning incremental refinements from its previous layer. Both primary object shapes and boundary details can be potentially better captured through the valuable mechanism brought by Res-Seg-Net. Exploring applications of Res-Seg-Net on more datasets, as well as the potential integrations of Res-Seg module with deep neural networks in other application areas, e.g., detection, are the directions of our future efforts.

5. REFERENCES

[1] Wei Wang, John A Ozolek, and Gustavo K Rohde, "Detection and classification of thyroid follicular lesions based on nuclear structure from histopathology images," *Cytometry Part A: The Journal of the International Society for Advancement of Cytometry*, vol. 77, no. 5, pp. 485–494, 2010.

[2] Hugo Borst, WOLFGANG Abmayr, and PETER Gais, "A thresholding method for automatic cell image segmentation.," *Journal of Histochemistry & Cytochemistry*, vol. 27, no. 1, pp. 180–187, 1979.

[3] Umesh Adiga, Ravi Malladi, Rodrigo Fernandez-Gonzalez, and C Ortiz de Solorzano, "High-throughput analysis of multispectral images of breast cancer tissue," *IEEE Transactions on Image Processing*, vol. 15, no. 8, pp. 2259–2268, 2006.

[4] Yuri Y Boykov and M-P Jolly, "Interactive graph cuts for optimal boundary & region segmentation of objects in nd images," in *Computer Vision, 2001. ICCV 2001. Proceedings. Eighth IEEE International Conference on*. IEEE, 2001, vol. 1, pp. 105–112.

[5] Jundong Liu, Charles D. Smith, and Hima Chebrolu, "Automatic multiple sclerosis detection based on integrated square estimation," in *IEEE, CVPR Workshops, 20-25 June, 2009*, 2009, pp. 31–38.

[6] Jonathan Long et al., "Fully convolutional networks for semantic segmentation," in *Proceedings of CVPR*, 2015, pp. 3431–3440.

[7] Olaf Ronneberger, Philipp Fischer, and Thomas Brox, "U-net: Convolutional networks for biomedical image segmentation," in *MICCAI*. Springer, 2015, pp. 234–241.

[8] Fisher Yu, Vladlen Koltun, and Thomas Funkhouser, "Dilated residual networks," in *Proceedings of the IEEE Conference on Computer Vision and Pattern Recognition*, 2017, pp. 472–480.

[9] Zhenli Zhang, Xiangyu Zhang, Chao Peng, Dazhi Cheng, and Jian Sun, "Exfuse: Enhancing feature fusion for semantic segmentation," *arXiv preprint arXiv:1804.03821*, 2018.

[10] Md Sarker, Mostafa Kamal, Hatem A Rashwan, Syeda Furruka Banu, Adel Saleh, Vivek Kumar Singh, Forhad UH Chowdhury, Saddam Abdulwahab, Santiago Romani, Petia Radeva, et al., "Slsdeep: Skin lesion segmentation based on dilated residual and pyramid pooling networks," *arXiv preprint arXiv:1805.10241*, 2018.

[11] Yishuo Zhang and Albert Chung, "Deep supervision with additional labels for retinal vessel segmentation task," *arXiv preprint arXiv:1806.02132*, 2018.

[12] Clément Playout, Renaud Duval, and Farida Cheriet, "A multitask learning architecture for simultaneous segmentation of bright and red lesions in fundus images," in *International Conference on Medical Image Computing and Computer-Assisted Intervention*. Springer, 2018, pp. 101–108.

[13] Yani Chen, Bibo Shi, Zhewei Wang, Pin Zhang, Charles D. Smith, and Jundong Liu, "Hippocampus segmentation through multi-view ensemble convnets," in *14th IEEE, ISBI 2017*, 2017, pp. 192–196.

[14] Yani Chen, Bibo Shi, Zhewei Wang, Tao Sun, Charles D. Smith, and Jundong Liu, "Accurate and consistent hippocampus segmentation through convolutional LSTM and view ensemble," in *Machine Learning in Medical Imaging*, 2017, pp. 88–96.

[15] Zengqiang Yan, Xin Yang, and Kwang-Ting Tim Cheng, "A deep model with shape-preserving loss for gland instance segmentation," in *International Conference on Medical Image Computing and Computer-Assisted Intervention*. Springer, 2018, pp. 138–146.

[16] Peter J Burt and Edward H Adelson, "The laplacian pyramid as a compact image code," in *Readings in Computer Vision*, pp. 671–679. Elsevier, 1987.

[17] Rebeca Marfil, Luis Molina-Tanco, Antonio Bandera, Juan Antonio Rodríguez, and F Sandoval, "Pyramid segmentation algorithms revisited," *Pattern Recognition*, vol. 39, no. 8, pp. 1430–1451, 2006.

[18] Philippe Thevenaz, Urs E Ruttimann, and Michael Unser, "A pyramid approach to subpixel registration based on intensity," *IEEE transactions on image processing*, vol. 7, no. 1, pp. 27–41, 1998.

[19] Kaiming He, Xiangyu Zhang, Shaoqing Ren, and Jian Sun, "Deep residual learning for image recognition," in *Proceedings of the IEEE conference on computer vision and pattern recognition*, 2016, pp. 770–778.

[20] Fausto Milletari et al., "V-net: Fully convolutional neural networks for volumetric medical image segmentation," in *3D Vision (3DV)*. IEEE, 2016, pp. 565–571.

[21] Peter Bankhead, Maurice B Loughrey, José A Fernández, Yvonne Dombrowski, Darragh G McArt, Philip D Dunne, Stephen McQuaid, Ronan T Gray, Liam J Murray, Helen G Coleman, et al., "Qupath: Open source software for digital pathology image analysis," *Scientific reports*, vol. 7, no. 1, pp. 16878, 2017.

[22] Moshe Shimrat, "Algorithm 112: position of point relative to polygon," *Communications of the ACM*, vol. 5, no. 8, pp. 434, 1962.